Modeling and optimization of solar-powered cascade Rankine cycle system with respect to the characteristics of steam screw expander

Pengcheng Li[a,b], Jing Li[a]*, Guangtao Gao[a], Gang Pei[a]*, Yuehong Su[c], Jie Ji[a], Bin Ye[b]

[a]*Department of Thermal Science and Energy Engineering, University of Science and Technology of China, 96 Jinzhai Road, Hefei, China*

[b]*School of automobile and traffic engineering, Hefei University of Technology, 193 Tunxi Road, Hefei, China*

[c]*Institute of Sustainable Energy Technology, University of Nottingham, University Park, Nottingham NG7 2RD, UK*

Abstract: The screw-type volumetric expander has great potential in distributed solar electric generating system (SEGS) applications regarding its ability of handling both steam and liquid. A parabolic trough collector (PTC)-coupled cascade thermodynamic system with the top screw expander (SE)-based steam Rankine cycle and the bottom turbine-based organic Rankine cycle (ORC) has the advantages of avoidance of superheater, and relatively low technical requirements in heat collection and storage. A significant characteristic of the solar cascade system is the highly off-design operation owing to the small built-in volume ratio ($r_{v,b}$) of SE. However, at present model on the system part-load behavior is lacked and the optimum working condition has yet to be determined. In this paper, an approximate SE over-expansion model is established, which reveals variation of SE isentropic efficiency with operating pressure ratio. Then off-design behavior of the whole system is modeled. The solar power efficiency on different conditions is investigated. Optimization of the system is conducted. Results indicate that the optimum hot side temperature ranges from about 499 K to 543 K when beam solar radiation (G_b) is 600-800 W/m^2. Maximum solar thermal power efficiency of 13.74-15.45% can be achieved in the situation of SE's $r_{v,b}$ of 5.0. The impact of low $r_{v,b}$ on power conversion is limited owing to SE good part-load behavior, and maximum efficiency of 13.12-15.11% is obtained when $r_{v,b}$ is 3.5. Annual optimization in Phoenix, Sacramento, Cape Town, Canberra, Lhasa and Barcelona is further implemented. The solar power output varies from 201.8 kWh/ m^2 to 347 kWh/ m^2 per year.

Keywords: screw expander; part-load behaviour; solar thermal power efficiency; built-in volume ratio

*Corresponding author. Tel. /Fax: +86 551 63601652. E-mail: lijing83@ustc.edu.cn, peigang@ustc.edu.cn

1. Introduction

Screw expander (SE) is a type of power equipment that utilizes exergy in working fluid of high temperature and pressure to generate electricity. Its working process consists of fluid admission, expansion and exhaust. SE possesses a number of advantages. First, unlike reciprocating piston expander, SE has all the moving parts rotate and hence can run at much higher speed. Second, unlike vane expander, the contact forces within SE are low, which makes it very reliable. Third, opposite to the scroll and rotary vane expanders, its sealing lines of contact that define the boundaries of each cell chamber, are of minimum length when the pressure within the working chamber is greatest. This minimizes the escape of fluid from the chamber due to leakage during the expansion process. Forth, the fluid velocities within it are roughly one order of magnitude smaller than those in turbo expander, and thus there is little risk of damage resulting from the admission of liquid/vapor mixtures. SE can admit fluids of any composition from pure liquid to dry vapor, while maintaining thermodynamic equilibrium between the phases [1].

Although at present SE is mainly employed in steam Rankine cycle-based industrial waste heat and geothermal power generation [2-4], it has great potential to be applied in solar electric generating systems (SEGSs) [5]. Compared with steam turbine-driven system, SEGS using SE eliminates superheater and is able to operate at relatively lower temperature and pressure, while maintaining an acceptable efficiency. In particular, by coupling SE steam Rankine cycle with a bottom organic Rankine cycle (ORC), higher solar thermal power conversion efficiency, simpler design of the expander and better reaction to low ambient temperature can be facilitated. The fundamental and structure of the SEGS using cascade steam-organic Rankine cycle (SORC) and steam SE have been introduced previously [5]. The system performance on given conditions of hot side temperature (473K/523K), cold side temperature (293K/313K) and SE efficiency (0.75/0.68) have been investigated.

A well-known characteristic of SE is the low built-in volume ratio ($r_{v,b}$). The commercial SEs generally have $r_{v,b}$ of about 2.5 to 6.0, while the steam volume ratio in practical plants with hot and cold side temperatures of 523 K and 303 K respectively may reach 200 or more. There is an appreciable mismatch between $r_{v,b}$ and the actual. Attributed to this characteristic, highly off-design operation of the SEGS is both inevitable and beneficial.

On the other hand, as a promising solar thermal power generation system, the off-design model of the SEGS has not been established yet. Without a mathematic model of the whole system at part-load operation, it is impossible to predict the optimum working conditions. So far most of the works have focused on the off-design model of SE itself. Modeling, performance prediction and experimental investigations have been carried out [6-9], and studies relevant to off-design operation of SE have been reported. $r_{v,b}$ and the operating pressure ratio (r_p) are two important variables in the off-design analysis. $r_{v,b}$ is set with SE design, influenced by the geometric shape, size, and flow feature. r_p equals to the quotient of evaporation pressure divided by the back pressure of discharge line, which is determined by operating conditions [10]. Avadhanula et al. built two empirical models for a SE based on experimental data. The SE isentropic efficiency varied gently when operating r_p ranged from 2.70 to 6.54 [11]. Hsu et al. experimentally investigated the performance of a SE-based ORC. The results demonstrated that the SE can be operated with a wide scope of supply pressure and operating r_p with satisfactory efficiency [12]. Papes et al. analyzed SE performance with computational fluid dynamics. They concluded that the operational power range of the expander could be largely increased in a variable hot side when opening additional inlet ports [13]. Read et al. focused on the optimization of the geometry of a twin SE for the expansion of wet steam. Close agreement was found between the predicted and measured results in large pressure difference across the expander [14]. Ng et al. put forward a thermodynamic model for SE by using some experimental data. For a SE with $r_{v,b}$ of 5, the drop of isentropic efficiency from the maximum was only 10% when the operating r_p increased by threefold as the built-in [15].

The above studies demonstrate a common feature of SE: The isentropic efficiency first increases sharply as the operating r_p ascends in the under-expansion process, and a maximum appears when operating r_p equals to the built-in, then it declines gently as the operating r_p rises continuously (i.e. over-expansion process). This implies SE is well suited to large pressure ratio/difference, while the drop of efficiency remains smooth. Both over- and under-expansion lead to undesirable effects in the cycle such as the "blowdown" and "blowback" phenomenon and hence result in loss of work production. According to Zhu et al., the correction factor (ratio of the actual expander net work to the available power at design) decreases faster in under-expansion condition than it does in over-expansion condition, therefore under-expansion should be avoided when adjusting a working condition, while slight over-expansion is acceptable [10].

Acknowledging the predecessors' works, equations for the part-load behavior of SE are accessible. By combing them with the heat collection and thermodynamic equations, mathematical formulas for the whole system under variable operating conditions can be derived. In this paper, it is the first time that off-design performance of the steam SE based-SEGS has been modeled. Thanks to the mathematical models, optimization of the system can be carried out via the following steps: First, heat-to-power conversion efficiency of the cascade cycle at variable ORC evaporation temperature is studied. The maximum efficiency of the cascade cycle at given hot side temperature (SRC evaporation temperature) is explored. Second, variation of the peak efficiency of the cascade cycle with the hot side temperature is investigated. Third, heat collection efficiency at variable hot side temperature is analyzed, and the maximum solar thermal electricity efficiency at given solar radiation can be found out. Fourth, variation of the maximum solar thermal electricity efficiency with solar radiation is examined. Therefore, the optimal SRC and ORC evaporation temperatures at different solar radiations can be determined. Finally, the annual power output in six areas is optimized. This work provides comprehensive information on the off-design performance and optimum operation of this kind of system.

2. System description

The PTC-direct steam generation (DSG) system with SORC is shown in Fig. 1. Cycle I (red colour) and Cycle Ⅱ (blue colour) are the steam Rankine cycle and ORC subsystems. Cycle I consists of SE, condenser (HX1), water pump (P1), heat storage unit with phase change materials (PCM) and PTC array. Cycle Ⅱ is comprised of turbine, condenser (HX2) and organic fluid pump (P2). HX1 serves as the evaporator for Cycle Ⅱ.

Due to the low heat storage temperature requirements in the SE-based SEGS, which is to be pointed out in Section 5.3, a variety of materials like water, conduction oil, solar salt (40%KNO_3 + 60%$NaNO_3$) and concrete are alternatives. However, heat storage is not the emphasis of this work and PCM is exemplified in the system.

Notably, compared with volumetric expander, turbine is able to handle higher volume ratio and has reached a much higher degree of technical maturity. By choosing isentropic or dry working fluid for the ORC, there is no need of superheat at the turbine inlet. Turbine may possess an efficiency of 80% even when the volume ratio reaches 50 [16, 17], and can compensate the influence of low $r_{v,b}$ of SE. From these viewpoints, turbine is employed in the bottom ORC.

3. Mathematical models

3.1. Expanders

There are four types of loss in SE operation: (i) loss due to mismatch of the r_p, (ii) fluid leakage loss, (iii) loss due to thermodynamic irreversibilities and (iv) mechanical friction loss from the rotating shaft. For each stage of the work loss, an efficiency term can be defined to account for it. They are theoretical, leakage, thermodynamic and mechanical efficiencies for (i)-(iv), respectively [15]. The actual overall isentropic efficiency can thus be defined as:

$$\varepsilon_{os} = \varepsilon_{Th}\varepsilon_{L}\varepsilon_{TM}\varepsilon_{M} = \varepsilon_{Th}\varepsilon_{D}\varepsilon_{M} \tag{1}$$

where
$$\varepsilon_{D} = \varepsilon_{L}\varepsilon_{TM} \tag{2}$$

ε_M is determined by the characteristic of SE, and it has a constant value for a specific SE. By definition, the theoretical efficiency is given as:

$$\varepsilon_{Th} = \frac{W_{TD}}{W_{TI}} = \frac{(1-{r_{v,b}}^{1-\gamma}) + (\gamma-1)(1-r_{v,b}/r_p)}{\gamma(1-{r_p}^{1-\gamma/\gamma})} \tag{3}$$

where γ is the isentropic index. It varies according to the working fluid and its state. γ is 1.13 for dry saturated steam.

$r_{v,b}$ is defined as

$$r_{v,b} = \frac{v_{out}}{v_{in}} \quad (4)$$

The thermodynamic work output W_{TM}, can be estimated by summing the shaft work output and the frictional work, i.e.

$$W_{TM} = W_S + W_F \quad (5)$$

where W_F is a direct function of the shaft speed N. It is generally assumed to be a constant if the rotation speed is unchanged. The diagram efficiency is given by the ratio of the thermodynamic work to the theoretical diagram work, i.e.

$$\varepsilon_D = \frac{W_{TM}}{W_{TD}} = \frac{W_s + W_F}{m_t P_{su} v_s \left[\frac{(1 - r_{v,b}{}^{1-\gamma})}{\gamma - 1} + (1 - \frac{r_{v,b}}{r_p}) \right]} \quad (6)$$

The definition of diagram efficiency includes the effect of leakage and thermodynamic irreversibility. The mass flow rate related to leakage in an expander can be estimated using the ideal-gas choked flow model with a given leakage flow area [18]. Therefore, it is expected that the expression of diagram efficiency is similar to that in the conventional turbomachines. The test results of the variation of diagram efficiency with r_p using dry saturated steam are shown in Fig. 2 [19]. It can be seen that large $r_{v,b}$ has a negligible effect on the diagram efficiency. At pressure ratio lower than 2.5, the diagram efficiency increases sharply with the decrement of r_p due to the presence of the blowback effect at the discharge phase. Although the diagram efficiency may be high at low values of r_p the amount of work output is small.

It is noteworthy that the diagram efficiency fluctuations in the range of high r_p

are gentle. The data is basically located near the magenta and blue straight lines, respectively. When r_p exceeds twice of the built in r_p, the diagram efficiency almost keeps constant.

Peak isentropic efficiency ($\varepsilon_{os,p}$) can be achieved when $\varepsilon_{Th,p}$ is 1.

$$\varepsilon_{os,p} = \varepsilon_{Th,p}\varepsilon_D\varepsilon_M \tag{7}$$

Combine Eqs. (1), (3) and (7), ε_{os} can be estimated as:

$$\varepsilon_{os} = \varepsilon_{os,p}\varepsilon_{Th} = \varepsilon_{os,p} \cdot \frac{\varepsilon_D}{\varepsilon_{D,p}} \frac{(1-r_{v,b}{}^{1-\gamma}) + (\gamma-1)(1-r_{v,b}/r_p)}{\gamma(1-r_p{}^{1-\gamma/\gamma})} \tag{8}$$

According to Eq. (8), the actual SE efficiency is affected by operating r_p, $\varepsilon_{os,p}$, $r_{v,b}$, working fluid and state.

The work generated by SE and turbine is defined as Eqs. (9) and (10):

$$W_{SE} = m_{\mathrm{I}}(h_1 - h_2) = m_{\mathrm{I}}(h_1 - h_{2s})\varepsilon_{os} \tag{9}$$

$$W_T = m_{\mathrm{II}}(h_5 - h_6) = m_{\mathrm{II}}(h_5 - h_{6s})\varepsilon_T \tag{10}$$

3.2. Collectors

A type of PTC installed in the USA with up to 2700 m^2 of aperture area is referenced here [20]. The performance formula of a single PTC provided by the manufacturer is [21]:

$$\eta_{PTC}(T) = 0.762 - 0.2125 \times \frac{T - T_a}{G_b} - 0.001672 \times \frac{(T - T_a)^2}{G_b} \tag{11}$$

where G_b is beam solar radiation (W/m^2); T is collector inlet temperature (K).

Hundreds of collectors are usually required in SEGS and the temperature difference between neighboring collectors is supposed to be small. It is reasonable to assume that the average operating temperature of the collector changes continuously from one module to another while calculating the overall collection efficiency.

Water in PTC experiences liquid phase and binary phase, and finally becomes saturated vapor. Collector efficiency in binary phase region can be calculated with Eq. (11) as the temperature remains constant. For liquid phase region, in order to reach an outlet temperature T_{out} with an inlet temperature T_{in}, the required aperture area is obtained by

$$A_l = \int_{T_{in}}^{T_{out}} \frac{m_{\mathrm{I}} \cdot C_p(T)}{\eta_{PTC}(T) \cdot G_b} dT \tag{12}$$

where m_{I} is mass flow rate of water in Cycle Ⅰ.

Heat capacity of water can be expressed by a first order approximation:

$$C_p(T) = C_{p,0} + \alpha(T - T_0) \tag{13}$$

Where $C_{p,0}$ is heat capacity corresponding to reference temperature T_0.

With $c_1 = 0.2125 / G_b$, $c_2 = 0.001672 / G_b$, the collector area according to Eqs. (11) - (13) is calculated by

$$A_l = \frac{m_{\mathrm{I}}}{c_2 G_b(\theta_2 - \theta_1)} \left[(C_{p,a} + \alpha\theta_1) \ln \frac{T_{out} - T_a - \theta_1}{T_{in} - T_a - \theta_1} + (C_{p,a} + \alpha\theta_2) \ln \frac{\theta_2 - T_{in} + T_a}{\theta_2 - T_{out} + T_a} \right] \tag{14}$$

where θ_1 and θ_2 are the arithmetical solutions of Eq. (15)（$\theta_1 < 0,\ \theta_2 > 0$）.

$$0.762 - c_1\theta - c_2\theta^2 = 0 \tag{15}$$

$$C_{p,a} = C_{p,0} + \alpha(T_a - T_0) \tag{16}$$

Collector efficiency in liquid phase region is calculated by

$$\eta_{PTC,l} = \frac{m_{\mathrm{I}} \Delta h_l}{G_b A_l} \tag{17}$$

Overall collector efficiency can be calculated by Eq. (18)

$$\eta_{PTC} = \frac{Q}{G_b(A_l + A_b)} = \frac{\Delta h_l + \Delta h_b}{\dfrac{\Delta h_l}{\eta_{PTC,l}} + \dfrac{\Delta h_b}{\eta_{PTC,b}}} \tag{18}$$

where Δh_l and Δh_b are the enthalpy increments of water in liquid phase and binary phase regions.

3.3. Heat exchanger

Heat balance in HX1 is expressed by Eq. (19):

$$m_{\mathrm{I}}(h_2 - h_3) = m_{\mathrm{II}}(h_5 - h_8) \tag{19}$$

$$T_3 - T_5 = T_{pp} \tag{20}$$

3.4. Pumps

The work required by pumps is expressed by

$$W_{p1} = m_{\mathrm{I}}(h_4 - h_3) = m_{\mathrm{I}}(h_{4s} - h_3) / \varepsilon_p \tag{21}$$

$$W_{p2} = m_{\mathrm{II}}(h_8 - h_7) = m_{\mathrm{II}}(h_{8s} - h_7) / \varepsilon_p \tag{22}$$

3.5. Thermal efficiency

Thermal efficiency (η_T) of the proposed system indicates how effectively solar radiation is converted into electricity.

$$\eta_T = \eta_{SORC} \cdot \eta_{PTC} = \frac{W_{net}}{G_b \cdot A} \tag{23}$$

where

$$\eta_{SORC} = \frac{W_{net}}{m_{\mathrm{I}}(h_1 - h_4)} \tag{24}$$

$$W_{net} = \left(W_{SE} + W_T\right) \cdot \varepsilon_g - \left(W_{p1} + W_{p2}\right) \tag{25}$$

3.6. Annual power output

The hourly weather data in EnergyPlus software is referenced [22], and the annual power generated can be calculated through multiplying the total heat collected by heat-to-power conversion efficiency.

$$W=\sum_{i=1}^{8760} G_{b,i}\cdot\eta_{PTC,i}\cdot\eta_{SORC,P}=\sum_{i=1}^{8760} Q_i\cdot\eta_{SORC,P} \tag{26}$$

4. Off-design performance of the cascade SORC

As turbine may have a large nominal pressure ratio and multi-stage expansion technology is mature, the structure of turbine can be more easily designed according to a specific working condition. Therefore turbine efficiency is taken as a fixed value and only part-load behavior of SE is focused on in this work.

4.1. Over-expansion performance of SE

Peak isentropic efficiency of SE is assumed to be 0.75 and only dry saturated steam is admitted to the expander inlet. Fixed parameters for calculation are listed in Table 1. In the previous work, it has been mentioned that an ORC evaporation temperature corresponding to theoretical maximum solar thermal power efficiency fails to provide a pressure ratio that matches the SE built-in r_p. The operating r_p shall be larger than the built-in for the sake of maximizing the cascade system efficiency [5]. Over-expansion of SE is beneficial. It leads to a slightly lower SE efficiency than the designed value but better thermodynamic performance of the whole system. Therefore, in this work, attention is paid to the SE behavior in the process of over-expansion rather than under-expansion.

The SE overall isentropic efficiency variation with r_p in over-expansion process is shown in Fig. 3. All the three curves decline gradually as the pressure ratio rises. The variation tendency is in consonance with the test results in references [11]-[15].

At the same pressure ratio, a larger $r_{v,b}$ leads to higher overall isentropic efficiency. Besides, the curve representative of larger $r_{v,b}$ is smoother, which indicates SE with larger $r_{v,b}$ has better part-load performance but is followed by higher cost. It's worth noting that Eq. (8) is an approximate over-expansion model and might be unable to offer high accuracy for extremely large r_p (>100).

For positive displacement machines, performance penalties associate with internal friction and vary with rotation speed. The best design of expander will hence involve a compromise between the needs for high speed to minimize leakage losses and for low speed to minimize friction losses, and for a large $r_{v,b}$ to minimize under-expansion losses and for a small $r_{v,b}$ to minimize the leakage effects while maximizing the mass flow and thereby keeping the size of the expander to a minimum [23, 24]. Since $r_{v,b}$ of commercial SE normally ranges from 2.5 to 6.0, two built-in volume ratios of 3.5 and 5 are exemplified in the following analysis.

4.2. Off-design performance of the cascade SORC

Given the hot side temperature (T_H) and cold side temperature (T_C), the cascade SORC efficiency shall first go up and then decrease with the reduction of ORC evaporation temperature (T_5) from T_H, and there exists an optimum ORC evaporation temperature, i.e. $T_{5,op}$. $T_{5,op}$ is the tradeoff between the irreversibilities in the SE and other elements of the SORC. It results in a lower SE efficiency than the design but higher degree of thermodynamic perfection of the SORC. Fig. 4 shows variation of $T_{5,op}$ with T_H when $r_{v,b}$ is 5. T_C is 313 K. For fluids of high critical temperature such as benzene and cyclohexane, optimum ORC evaporation temperatures exhibit almost linear growth as T_H climbs. For fluids of moderate critical temperature such as R141b, pentane, R365mfc and R123, their curves first ascend approximately linearly and then approach to the values of corresponding critical temperatures gently when T_H is above 603 K. For fluids of low critical temperature such as R245fa, butane, isobutene and R236ea, their optimum ORC evaporation temperatures first raise slowly, and then they will remain stable at temperatures close to the corresponding critical temperatures when T_H is above 563 K.

Fig. 5 shows variation of $T_{5,op}$ with T_H when $r_{v,b}$ is 3.5. Similar to Fig. 4, $T_{5,op}$ representing benzene and cyclohexane is in nearly direct proportion to T_H. For R141b, pentane, R365mfc and R123, their curves first ascend roughly linearly and then approach to the values of corresponding critical temperatures mildly when T_H is above 583 K. The slopes of the rest four curves are small and $T_{5,op}$ gets close to the corresponding critical temperatures when T_H is higher than 543 K. Meanwhile, $T_{5,op}$ in Fig. 5 is generally higher than that in Fig. 4 for the same fluid and T_H. It manifests in the case of $r_{v,b}$ is 3.5, the temperature difference driving the bottom ORC would be larger, accompanied by larger design volume ratio, more complicated and relatively higher cost turbine.

The phenomenon in Figs. 4 and 5 can be explained as follows: for many organic fluids, ORC efficiency will increase slightly or even decrease when the evaporation temperature is near the critical point, which can be manifested by Fig. 6. Single stage ORC is taken as example. Efficiencies of turbine and pump are 0.75 and 0.8, respectively. Condensation temperature is 313 K. Benzene and cyclohexane have relatively high critical temperature which are beyond the scale of the horizontal axis. Turning points on the curves can be seen for most fluids. As a result, $T_{5,op}$ of most fluids in the cascade cycle are close to their critical temperatures. Because only subcritical cycle is considered in this work, the curves in Figs. 4 and 5 no longer move up once the critical temperature of a fluid is achieved.

Figs. 7 and 8 show variation of peak efficiency of the cascade cycle (η_{SORC}) with T_H when built-in volume ratio is 5 and 3.5, respectively. Each point represents optimized cascade cycle efficiency with a corresponding $T_{5,op}$ at each T_H. Peak η_{SORC} first shows parabolic growth and then descends as T_H rises for all the fluids in both figures. Given T_H, benzene exhibits the highest optimum η_{SORC} while R236ea displays the lowest. Maxima range from 23.55% to 28.74% when $r_{v,b}$ is 5 and from 22.17% to 28.12% when $r_{v,b}$ is 3.5. The corresponding hot side temperatures range from 593 K to 633 K in Fig. 7 and from 583 K to 623 K in Fig. 8 as depicted by two red dotted lines. Besides, peak η_{SORC} in Fig. 8 is about 0.31-1.48% lower than that in Fig. 7 for the same fluid and T_H. The decrement of peak η_{SORC} is limited on account of good SE part-load performance. In conclusion, higher peak η_{SORC} can be obtained and simpler ORC turbine is suggested in the case of higher $r_{v,b}$ of SE. SE with lower $r_{v,b}$ and less cost is also applicative, but with drawbacks of marginally lower peak η_{SORC} and a bit more complex ORC turbine.

Figs. 7 and 8 illustrate the peak η_{SORC} can fall down as T_H moves up. The reason is disclosed by Fig. 9, in which SE-based single stage steam Rankine cycle is exemplified. $r_{v,b}$ is 5 and the condensation temperature is 313 K. It can be seen that steam Rankine cycle efficiency first increases and then decreases as the evaporation temperature rises, while SE efficiency (ε_{0S}) declines unceasingly. In regard to the characteristics of SE, the cycle efficiency is not a monotone increasing function of T_H. The output work can be viewed as the product of technical work ($-\int_{p_{in}}^{p_{out}} v\mathrm{d}p$) and ε_{0S}. The expander has high ε_{0S} at pressure near the built-in. With the increment in T_H, the integral interval of pressure is enlarged, which has positive effect on the output work. On the other hand, the specific volume at the expander inlet drops, and the expander becomes less efficient during fluid expansion in the lower pressure range. This is the negative effect on the power conversion. At low T_H, the positive effect seems to play a dominant role and the cycle efficiency mounts up as T_H increases. At high T_H, the opposite is true and SE works in extremely off-design condition. The negative effect is more important and the efficiency goes down.

5. Optimization of the solar-powered cascade system

5.1. Optimization of solar power efficiency at different hot side temperatures

Fig. 10 shows η_T varying with T_5 when $r_{v,b}$ is 5 and T_H is 473 K. G_b is 800 W/m^2 and ambient temperature (T_a) is 303 K. Ten organic fluids are adopted in the bottom ORC. A higher T_5 corresponds to smaller temperature difference in the top steam Rankine cycle and thus lower operating r_p in SE when T_H and T_C are fixed. All the ten curves open downward. For each curve, there is a T_5 at which η_T reaches the maximum, i.e. $T_{5,op}$. $T_{5,op}$ ranges from 379 K to 390 K as depicted by two red dotted lines in the figure.

To provide an operating volume ratio of steam SE equal to the built-in, the ORC evaporation temperature shall be 396 K, which is the characteristic ORC evaporation temperature ($T_{5,ch}$). $T_{5,ch}$ is the T_5 that minimizes the thermodynamic irreversibility in the SE. However, the thermodynamic irreversibility in other elements of the system at $T_{5,ch}$ is larger than that at $T_{5,op}$. The deviation of $T_{5,op}$ from $T_{5,ch}$ is about 6-17 K. The deviation varies with different organic fluids and higher η_T results in smaller deviation.

Figs. 11 and 12 illustrate η_T varying with T_5 when $r_{v,b}$ and T_H are 5 and 523 K, 5 and 573 K, respectively. G_b is maintained at 800 W/m^2. $T_{5,op}$ rises as T_H is elevated, which ranges from 401 K to 419 K in Fig. 11 and from 412 K to 446 K in Fig. 12. In addition, the deviation of $T_{5,op}$ from $T_{5,ch}$ becomes enlarged, which is about 11-29 K in Fig. 11 and 17-51 K in Fig. 12. Higher T_H causes greater off-design operation of SE. For some fluids of low critical temperature, optimum ORC evaporation temperatures are close to their critical temperatures at high T_H, for instance R245fa, butane, isobutene and R236ea in Fig. 12.

It can be observed that in all the three cases, benzene and R236ea present the highest and lowest peak efficiencies, respectively. In particular, the peak solar thermal power efficiency ($\eta_{T,P}$) when T_H is 573 K is 0.02-0.71% lower than that when T_H is 523 K, which manifests 573 K may not be the optimum T_H for the cascade system. Furthermore, an evaporation temperature of 573 K corresponds to a saturation steam pressure of 8.57 MPa. As the shell casing of SE is mostly made up of steel, an inlet pressure higher than 5 MPa will not be applicable due to the current limitation of mechanical pressure-bearing ability.

Fig. 13 illustrates variation of $\eta_{T,P}$ with T_H when $r_{v,b}$ is 5. Each point stands for optimized solar thermal power efficiency at each T_H. The flowchart of optimization is shown in Fig. 14. All the efficiency curves first increase and then decrease. The maxima vary from 13.74% to 15.45% and are approximatively located on the red dotted line. The optimal T_H ranges from 520 K to 543 K for different ORC fluids. By comparison with Fig. 7, the optimum T_H for each fluid in the SEGS gets appreciably lower than that of the cascade SORC in the absence of solar collectors. And the decrement may exceed 70-80 K.

Fig. 15 shows variation of peak solar thermal power efficiency with T_H when $r_{v,b}$ is 3.5. The maxima vary from 13.12% to 15.11% and the optimal T_H ranges from 510 K to 540 K. Both $\eta_{T,P}$ and the optimal T_H declines with the decrement in $r_{v,b}$. However, the adverse impact of low $r_{v,b}$ on system power efficiency is limited on account of good SE part-load behavior.

5.2. Optimization of solar power efficiency at different beam solar radiations

Fig. 16 shows variation of optimum T_H with G_b when $r_{v,b}$ is 5. All the ten curves increase drastically with the increment in G_b in the low interval (< 600 W/m^2) and then go up slowly when G_b is stronger. The range of optimum T_H is 441-451 K when G_b is 300 W/m^2 and 523-550 K when G_b is 900 W/m^2. The difference between optimum T_H of any two fluids extends as G_b is enhanced. Benzene and R236ea present the highest and lowest optimum T_H at the same G_b, respectively.

Fig. 17 shows variation of maximum solar thermal power efficiency with G_b when $r_{v,b}$ is 5. Maximum power efficiency shows parabolic growth as G_b rises.

The range of maximum power efficiency is 10.21-10.83% when G_b is 300 W/m^2 and 14.08-15.98% when G_b is 900 W/m^2. The maximum power efficiency is broadened with increasing G_b. Benzene exhibits the highest maximum power efficiency while R236ea displays the lowest at the same G_b.

5.3. Annual T_H optimization in different areas

R123 is adopted as the ORC fluid in annual T_H optimization for the following reasons: First, R123 is nonflammable and the safety level is A1. Its global warming potential is low and ozone depletion potential is close to zero. It will not be phased out until 2030 under current legislation. Although it is less efficient than benzene, the latter is inflammable, toxic and the safety level is B2. Second, R123 is widely used in ORC research both theoretically [25-27] and experimentally [28-33]. Third, the saturation pressure of benzene is much lower than R123's at low ambient temperature. For instance, the saturation pressure at 303 K is 0.016 MPa and 0.109 MPa for benzene and R123 respectively. The high vacuum in the condenser not only requires strict mechanical seal technology, but also has negative impact on cycle efficiency [34]. Fourth, the maximum efficiency relative decrement of R123 as compared with that of benzene is quite slight, which is 1.8-5.9% according to Fig. 17.

The annual T_H optimization should be based on the fact that normally the expanders operate at constant temperature though irradiation varies from time to time in areas and the heat storage material is unlikely to be replaced all the year round. Therefore, once T_H is assigned the expander and heat storage material can be designed accordingly. This T_H is kept constant for year-round operation [35]. To achieve the maximum annual power output, optimization is conducted at different T_H. A SE with $r_{v,b}$ of 5 is selected. The processes of heat collection and power generation are simultaneous. Fig. 18 shows annual output of the solar thermal electric power generation with T_H. The flowchart of optimization is shown in Fig. 19. The power output first increases and then goes down marginally. The optimal hot side temperatures and the corresponding electricity outputs for different areas are: Phoenix 533 K, 347 kWh/m^2; Sacramento 523 K, 291.2 kWh/m^2; Cape Town 513 K, 248.8 kWh/m^2; Canberra 513 K, 223.5 kWh/m^2; Lhasa 493 K, 209.5 kWh/m^2; Barcelona 503 K, 201.8 kWh/m^2.

The optimal T_H varies within range of 493-533 K in these areas, which is beneficial to PTC system design. First, a hot side temperature higher than 533 K results in decline of power efficiency and higher expander inlet pressure (with saturation pressure above 4.68 MPa). This leads to longer payback period for the power plant and higher technical requirements for SE. Second, 493-533 K is favorable for heat collection in the solar field. PTC-DSG plant based on steam turbine is not widely applied nowadays, partially due to the high temperature and pressure (usually more than 673 K and 10 MPa) in the collector tubes. Owing to the thoroughly different properties of metal and glass (e.g. thermal expansion coefficient and wettability), sealing failure/degradation of the receiver may be caused when the operating temperature fluctuates from nearly 673 K at daytime to 300 K at night. In contrast, temperature about 510 K and pressure around 3.1 MPa are sufficient for the power conversion of SE-based cascade system. The sealing failure/degradation can be eliminated on account of much smaller operating temperature fluctuation throughout day and night. Meanwhile, the difficulties such as high accurate tracking system, frequent maintenance, repair/replacement of moving parts and gears associated with large concentration ratio (usually ranges from 80 to 100) in conventional turbine-based PTC plants can be eased. Third, easier thermal storage is facilitated. The problems associated with limited PCMs, flammability and thermal instability of mineral oil and high pressure steam vessel in conventional turbine-based SEGSs can be overcome.

6. Conclusion

Screw expander (SE)-based PTC-DSG system with cascade SORC has many advantages and is one promising SEGS technology. The highly off-design operation of SE is the most substantial feature of the cascade system. A quantitative analysis of the part-load behavior of SE as well as the whole system is performed in this work. Parametric optimization is further carried out. Following conclusions are drawn:

Given the hot side temperature (T_H), there is an optimum ORC evaporation temperature ($T_{5,op}$) in the cascade Rankine cycle. $T_{5,op}$ is correlated with T_H and their relationship depends on the sort of ORC fluid used. For fluids of high critical temperature like benzene, $T_{5,op}$ is almost proportional to T_H. For fluids of low critical temperature such as R245fa, $T_{5,op}$ first experiences smooth increment as T_H ascends, and then it will remain relatively constant at temperature close to the fluid critical point. No significant increment in $T_{5,op}$ is observed at higher T_H.

The peak cascade cycle efficiency (η_{SORC}) is no longer a monotone increasing function of T_H regarding the small built-in volume ratio ($r_{v,b}$) and part-load behavior of SE. The reason behind this uncommon phenomenon is that higher T_H could lead to lower specific volume at the expander inlet and degraded expander performance. There exists a maximum η_{SORC} for each fluid. For the ten fluids investigated, maxima range from 23.55% to 28.74% when $r_{v,b}$ is 5 and from 22.17% to 28.12% when $r_{v,b}$ is 3.5. The corresponding T_H varies from about 590 K to 630 K, with the minimum and maximum values for R236ea and benzene, respectively.

Maximum solar thermal power efficiency of 13.74-15.45% can be achieved on the condition of SE $r_{v,b}$ of 5.0 and G_b of 800 W/m^2. The optimal T_H ranges from 520 K to 543 K, which is lower than that of the cascade cycle without solar collectors. Maximum power efficiency of 13.12-15.11% is achieved in the situation of $r_{v,b}$ of 3.5, with optimal T_H ranging from 510 K to 540 K. Benzene and R236ea show the highest and lowest efficiencies among the ten ORC fluids. Low $r_{v,b}$ shows minor adverse impact on power efficiency owing to good performance of the SE under part-load conditions. On the other hand, both optimum T_H and $\eta_{T,p}$ are influenced remarkably by G_b.

Annual optimization of T_H of the SEGS in six regions with abundant beam radiation resources is carried out. The T_H in these regions ranges from 493 K to 533 K, which is obviously lower than that in the mainstream turbine-based SEGSs. The yearly power output from 201.8 kWh/ m^2 to 347 kWh/ m^2 is obtained. The SORC using steam SE is a good match to the PTC and thermal storage material. The design and selection of solar energy collection and storage technologies will benefit from the relatively low operating temperature and pressure of SORC.

Acknowledgment

This study was sponsored by the National Science Foundation of China (NSFC 51476159 and 51206154), Dongguan Innovative Research Team Program (No. 2014607101008), National Science and Technology Support Program (No. 2015BAD19B02) and Project of EU Marie Curie International Incoming Fellowships (703746).

REFERENCES

[1] I.K. Smith, N. Stosic, A. Kovacevic. Power Recovery From Low Grade Heat by Means of Screw Expanders. Elsevier 2014.

[2] Engineering case. Available from: www.jxhdep.com/en/newsInfo.asp?pid=4.

[3] Helix Power SEs. Available from: www.heliexpower.com/category/news.

[4] Opcon's SEs. Available from: www.opcon.se/web/oes_en.aspx.

[5] Jing Li, Pengcheng Li, Gang Pei, Jahan Zeb Alvi, Jie Ji. Analysis of a novel solar electricity generation system using cascade Rankine cycle and steam screw expander. Applied Energy 2016; 165: 627-638.

[6] A. Kovacevic, N. Stosic, I.K. Smith, E. Mujic. Advances in numerical modelling of helical screw machines. International Compressor Engineering Conference at Purdue 2010.

[7] H. Leibowitz, I.K. Smith, N. Stosic. Cost effective small scale ORC systems for power recovery from low grade hot sides. ASME 2006 International Mechanical Engineering Congress and Exposition, American Society of Mechanical Engineers 2006: 521-527.

[8] Hao Tang, Huagen Wu, Xiaolin Wang, Ziwen Xing. Performance study of a twin-screw expander used in a geothermal organic Rankine cycle power generator. Energy 2015; 90: 631-642.

[9] D. Ziviani, M. van den Broek, M. De Paepe. Geometry-based Modeling of Single Screw Expander for Organic Rankine Cycle Systems in Low-grade Heat Recovery. Energy Procedia 2014; 61: 100-103.

[10] Yadong Zhu, Liang Jiang, Victor Jin, Lijun Yu. Impact of built-in and actual expansion ratio difference of expander on ORC system performance. Applied Thermal Engineering 2014; 71: 548-558.

[11] Vamshi Krishna Avadhanula, Chuen-Sen Lin. Empirical models for a screw expander based on experimental data from organic Rankine cycle system testing. Journal of Engineering for Gas Turbines and Power 2014; 136: 062601.

[12] Sung-Wei Hsu, Hsiao-Wei D. Chiang, Chih-Wei Yen. Experimental investigation of the performance of a hermetic screw-expander organic Rankine cycle. Energies 2014; 7: 6172-6185.

[13] Iva Papes, Joris Degroote, Jan Vierendeels. New insights in twin screw expander performance for small scale ORC systems from 3D CFD analysis. Applied Thermal Engineering 2015; 91: 535-546.

[14] Matthew Read, Nikola Stosic, Ian K. Smith. Optimization of Screw Expanders for Power Recovery From Low-Grade Hot sides. Energy Technology & Policy 2014; 1: 131-142.

[15] K. C. NG, T. Y. Bong, T. B. Lim. A thermodynamic model for the analysis of screw expander performance. Heat Recovery Systems and CHP 1990; 10: 119-133.

[16] Costante Invernizzia, Paolo Ioraa, Paolo Silva. Bottoming micro-Rankine cycles for micro-gas turbines. Applied Thermal Engineering 2007; 27: 100-110.

[17] Gequn Shu, Xiaoning Li, Hua Tian, Xingyu Liang, Haiqiao Wei, Xu Wang. Alkanes as working fluids for high-temperature exhaust heat recovery of diesel engine using organic Rankine cycle. Applied Energy 2014; 119: 204-217.

[18] Gordon F.C. Rogers, Y. R. Mayhew. Engineering Thermodynamics—Heat and Work Transfer. ELBS Book 1964.

[19] Botan Koto-Ku. Screw type steam engine. Internal report of Mayekawa Mfg Co Ltd. 2-3-1 1984; Tokyo 135, Japan.

[20] Dirk Krueger, Alfred Heller, Klaus Hennecke, Karsten Duer. Parabolic trough collectors for district heating systems at high latitudes: a case study. In: Proceedings of Eurosun 2000.

[21] Soteris A. Kalogirou. Solar thermal collectors and applications. Progress in energy and combustion science 2004; 30: 231-295.

[22] US Department of Energy, 2008. Available from: http://apps1.eere.energy.gov/buildings/energyplus/cfm/weather_data.cfm.

[23] I.K. Smith, N.R. Stosic. Deriving mechanical power by expanding a liquid to its

vapour. US Patents 1998.

[24] I.K. Smith, N. Stošič, C.A. Aldis. Development of the Trilateral Flash Cycle System: Part 3: The Design of High-Efficiency Two-Phase Screw Expanders, Proceedings of the Institution of Mechanical Engineers, Part A: Journal of Power and Energy 1996; 210: 75-93.

[25] Gang Pei, Jing Li, Jie Ji. Design and analysis of a novel low-temperature solar thermal electric system with two-stage collectors and heat storage units. Renewable Energy 2011; 36: 2324-2333.

[26] Man Wana, Jiangfeng Wang, Yuzhu Zhao, Pan Zhao, Yiping Dai. Thermodynamic analysis and optimization of a solar-driven regenerative organic Rankine cycle (ORC) based on flat-plate solar collectors. Applied Thermal Engineering 2013; 50: 816-825.

[27] Gequn Shu, Jian Zhao, Hua Tian, Xingyu Liang, Haiqiao Wei. Parametric and exergetic analysis of waste heat recovery system based on thermoelectric generator and organic rankine cycle utilizing R123. Energy 2012; 45: 806-816.

[28] Ye-Qiang Zhang, Yu-Ting Wu, Guo-Dong Xia, Chong-Fang Ma, Wei-Ning Ji, Shan-Wei Liu, Kai Yang, Fu-Bin Yang. Development and experimental study on organic Rankine cycle system with single-screw expander for waste heat recovery from exhaust of diesel engine. Energy 2014; 77: 499-508.

[29] Naijun Zhou, Xiaoyuan Wang, Zhuo Chen, Zhiqi Wang. Experimental study on Organic Rankine Cycle for waste heat recovery from low-temperature flue gas. Energy 2013; 55: 216-225.

[30] Maoqing Li, Jiangfeng Wang, Weifeng He, Lin Gao, Bo Wang, Shaolin Ma, Yiping Dai. Construction and preliminary test of a low-temperature regenerative Organic Rankine Cycle (ORC) using R123. Renewable Energy 2013; 57: 216-222.

[31] Gang Pei, Jing Li, Yunzhu Li, Dongyue Wang, Jie Ji. Construction and dynamic test of a small-scale organic rankine cycle. Energy 2011; 36: 3215-3223.

[32] Jing Li, Gang Pei, Yunzhu Li, Jie Ji. Evaluation of external heat loss from a small-scale expander used in organic Rankine cycle. Applied Thermal Engineering 2011; 31: 2694-2701.

[33] Jing Li, Gang Pei, Yunzhu Li, Dongyue Wang, Jie Ji. Energetic and exergetic investigation of an organic Rankine cycle at different hot side temperatures. Energy 2012; 38: 85-95.

[34] Jing Li, Gang Pei, Yunzhu Li, Dongyue Wang, Jie Ji. Examination of the expander leaving loss in variable organic Rankine cycle operation. Energy Conversion and Management 2013; 65: 66-74.

[35] Li Jing, Pei Gang, Ji Jie. Optimization of low temperature solar thermal electric generation with Organic Rankine Cycle in different areas. Applied Energy 2010; 87: 3355-3365.

Figure Legend

Fig. 1. Schematic diagram of the PTC-SORC system with DSG

Fig. 2. Variation of diagram efficiency with pressure ratio using dry saturated steam: test result by Ku et al. [15]

Fig. 3. Variation of overall isentropic efficiency with pressure ratio

Fig. 4. Variation of $T_{5,op}$ with T_H when $r_{v,b}$ is 5.

Fig. 5. Variation of $T_{5,op}$ with T_H when $r_{v,b}$ is 3.5.

Fig. 6. Variation of ORC efficiency with evaporation temperature.

Fig. 7. Variation of peak η_{SORC} with T_H when $r_{v,b}$ is 5.

Fig. 8. Variation of peak η_{SORC} with T_H when $r_{v,b}$ is 3.5.

Fig. 9. Variations of steam Rankine cycle and screw expander efficiencies with evaporation temperature.

Fig. 10. Variation of solar thermal power efficiency with T_5 when $r_{v,b}$ is 5 and T_H is 473 K.

Fig. 11. Variation of solar thermal power efficiency with T_5 when $r_{v,b}$ is 5 and T_H is 523 K.

Fig. 12. Variation of solar thermal power efficiency with T_5 when $r_{v,b}$ is 5 and T_H is 573 K.

Fig. 13. Variation of peak solar thermal power efficiency with T_H when $r_{v,b}$ is 5.

Fig. 14. Determination of peak solar thermal power efficiency with T_H.

Fig. 15. Variation of peak solar thermal power efficiency with T_H when $r_{v,b}$ is 3.5.

Fig. 16. Variation of optimum hot side temperature with G_b when $r_{v,b}$ is 5.

Fig. 17. Variation of maximum solar thermal power efficiency with G_b when $r_{v,b}$ is 5.

Fig. 18. Annual output of the solar thermal electric power generation with T_H.

Fig. 19. Determination of maximum annual power output with T_H.

Table legend

Table 1. Fixed parameters for calculation.

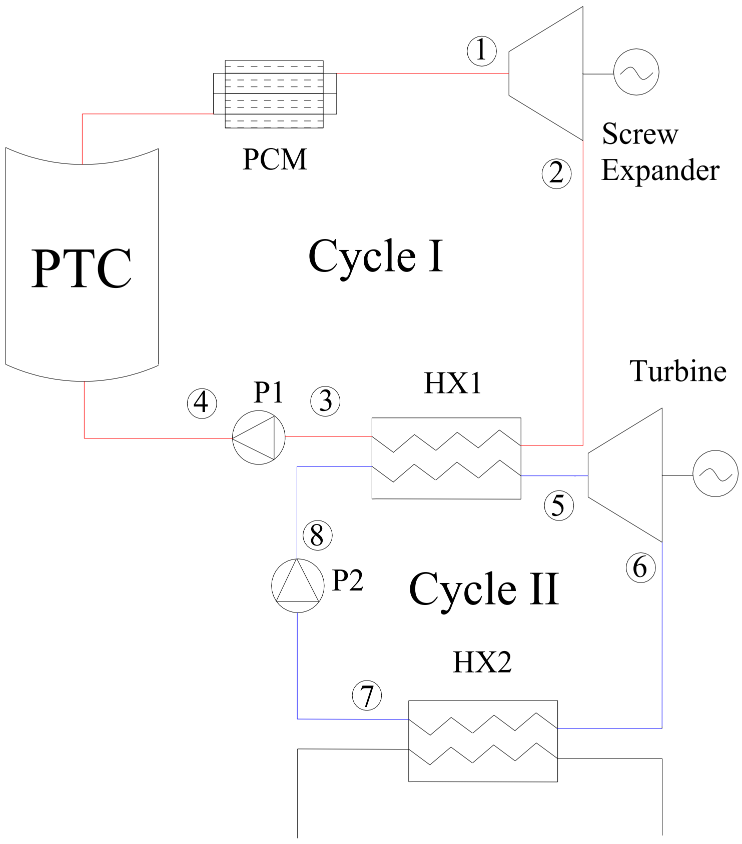

Fig. 1. Schematic diagram of the PTC-SORC system with DSG.

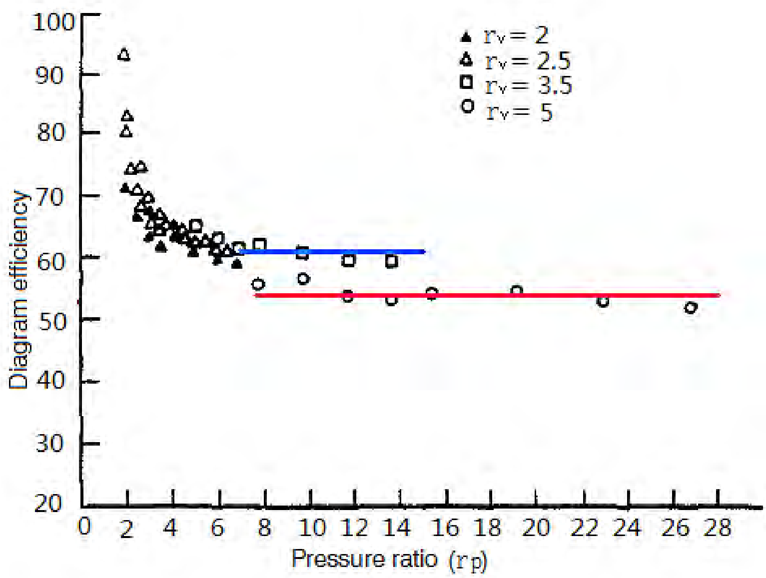

Fig. 2. Variation of diagram efficiency with pressure ratio using dry saturated steam: test result by Ku et al. [15].

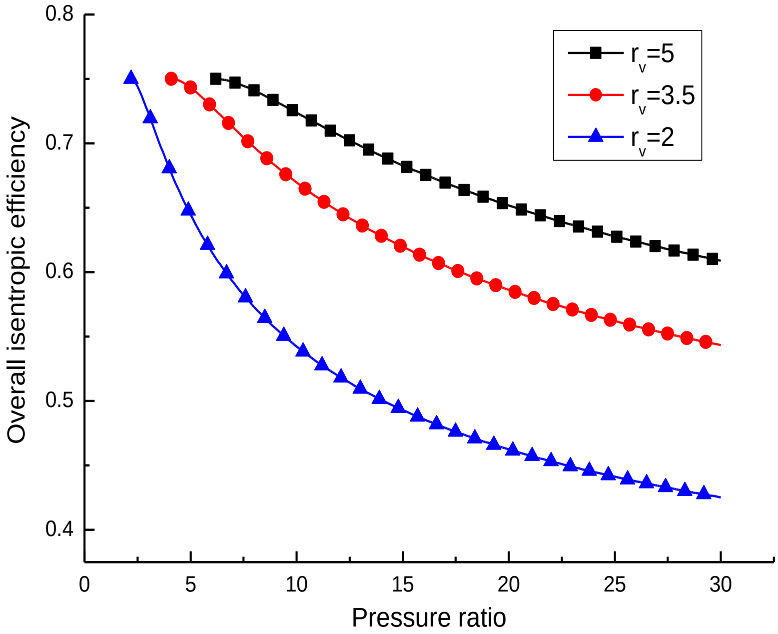

Fig. 3. Variation of overall isentropic efficiency with pressure ratio.

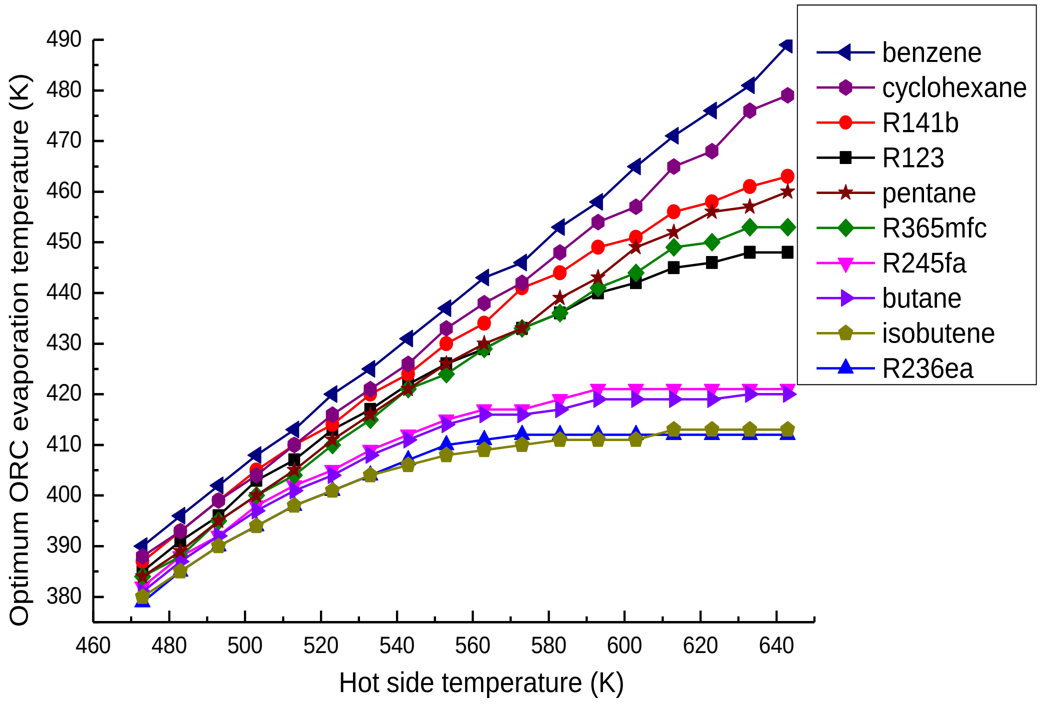

Fig. 4. Variation of $T_{5,op}$ with T_H when $r_{v,b}$ is 5.

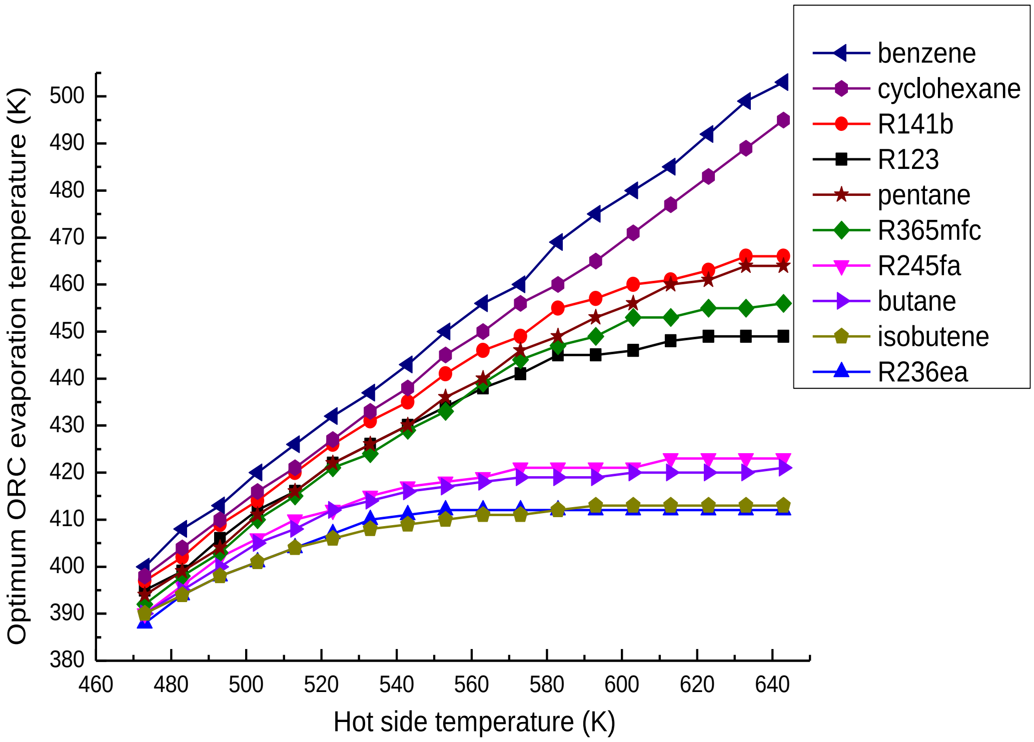

Fig. 5. Variation of $T_{5,op}$ with T_H when $r_{v,b}$ is 3.5.

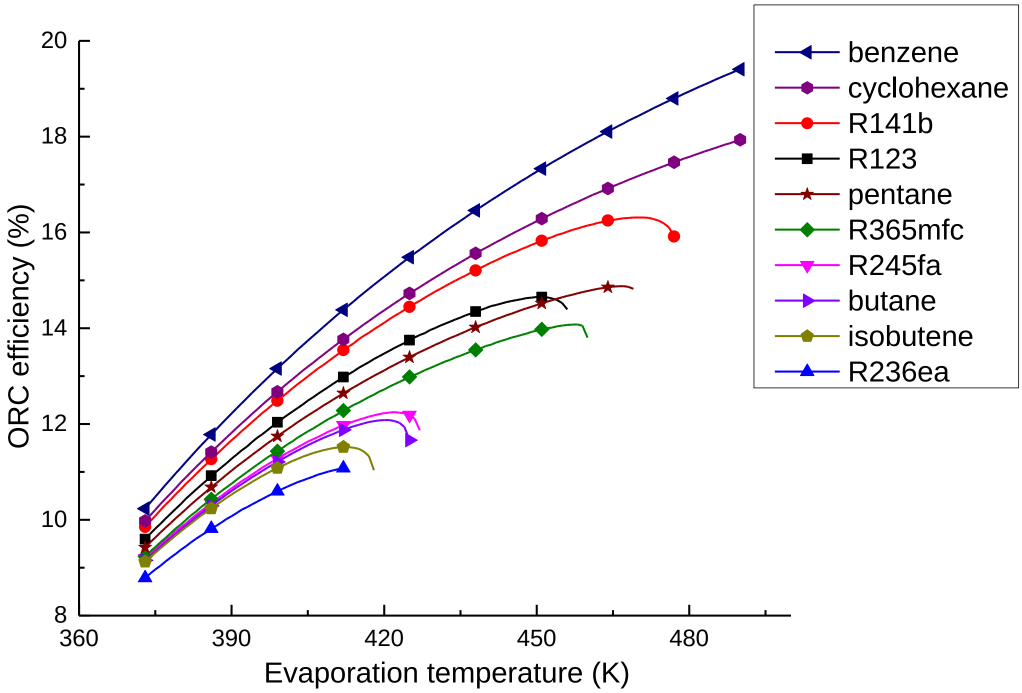

Fig. 6. Variation of ORC efficiency with evaporation temperature.

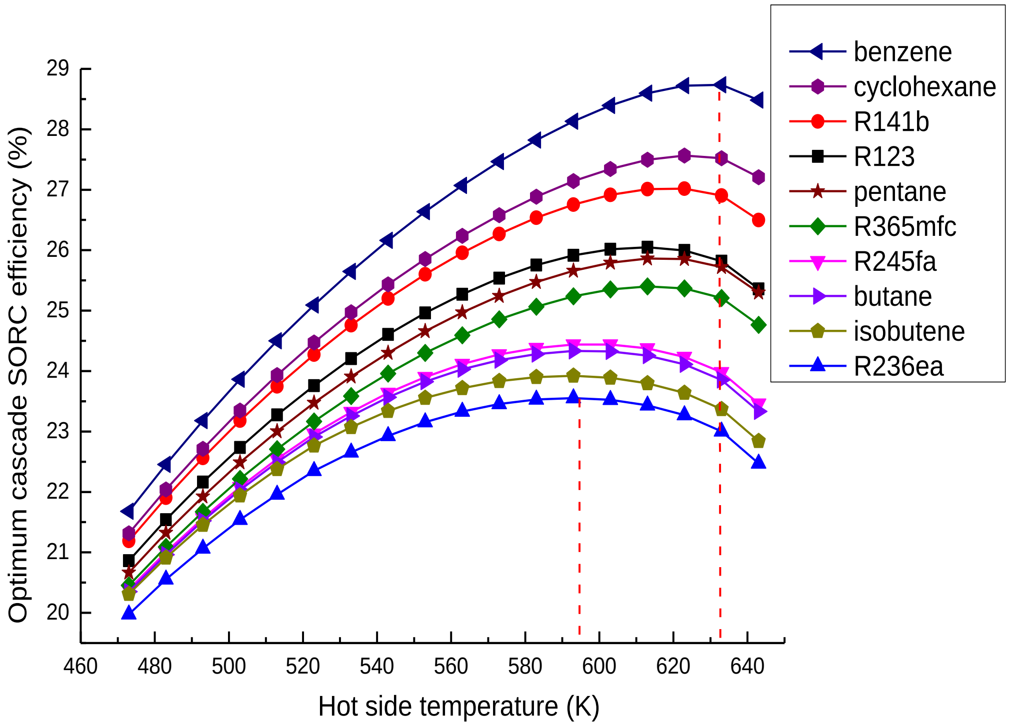

Fig. 7. Variation of peak η_{SORC} with T_H when $r_{v,b}$ is 5.

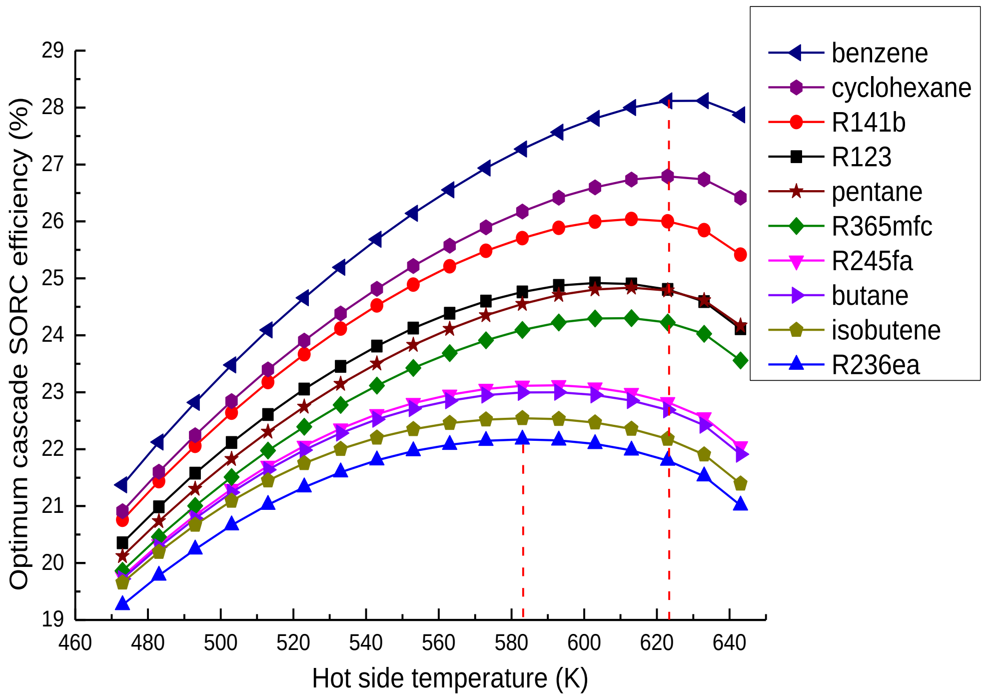

Fig. 8. Variation of peak η_{SORC} with T_H when $r_{v,b}$ is 3.5.

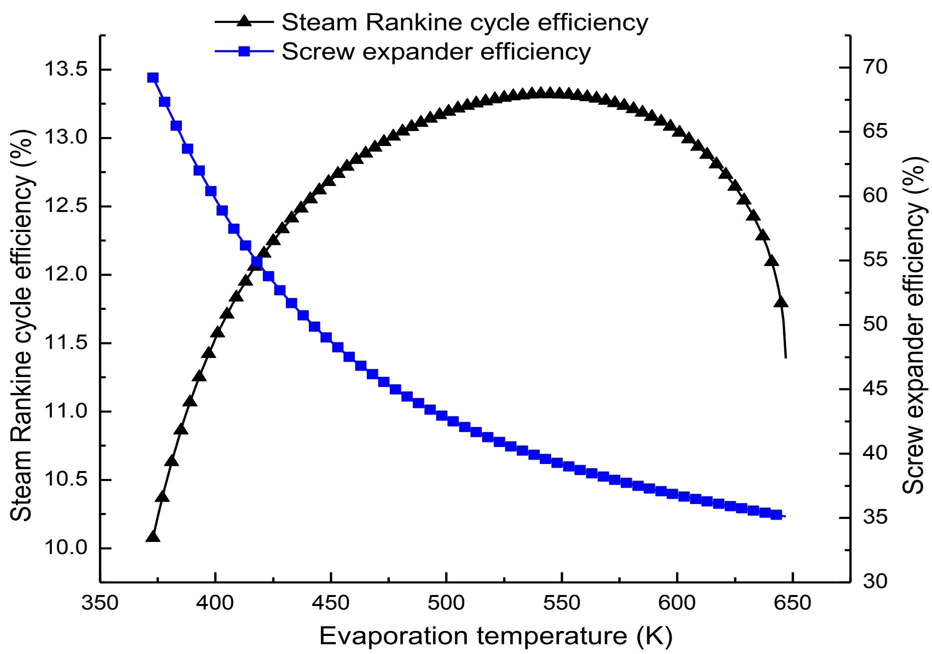

Fig. 9. Variations of steam Rankine cycle and screw expander efficiencies with evaporation temperature.

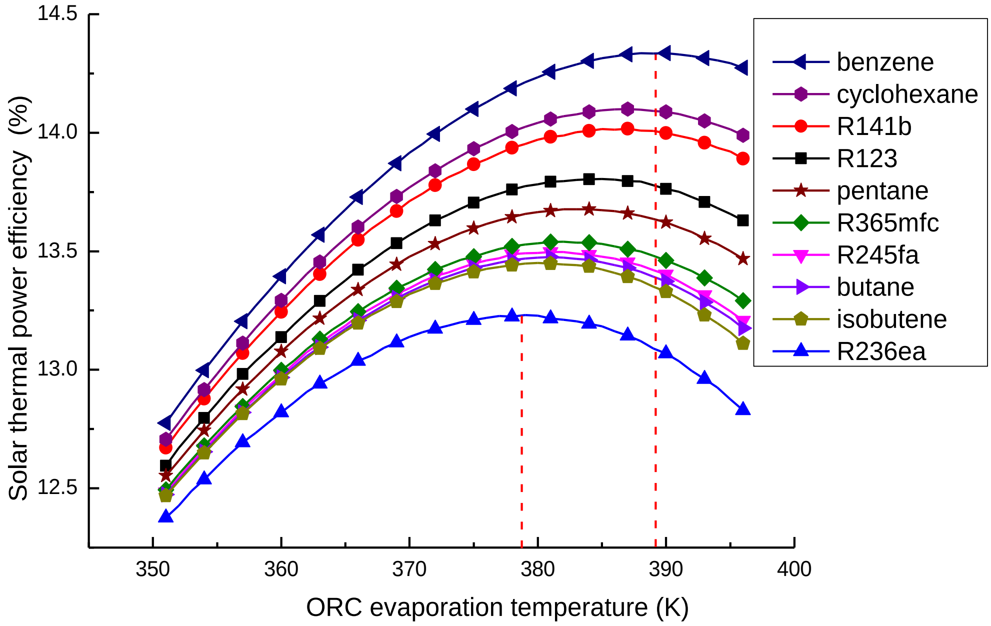

Fig. 10. Variation of solar thermal power efficiency with T_5 when $r_{v,b}$ is 5 and T_H is 473 K.

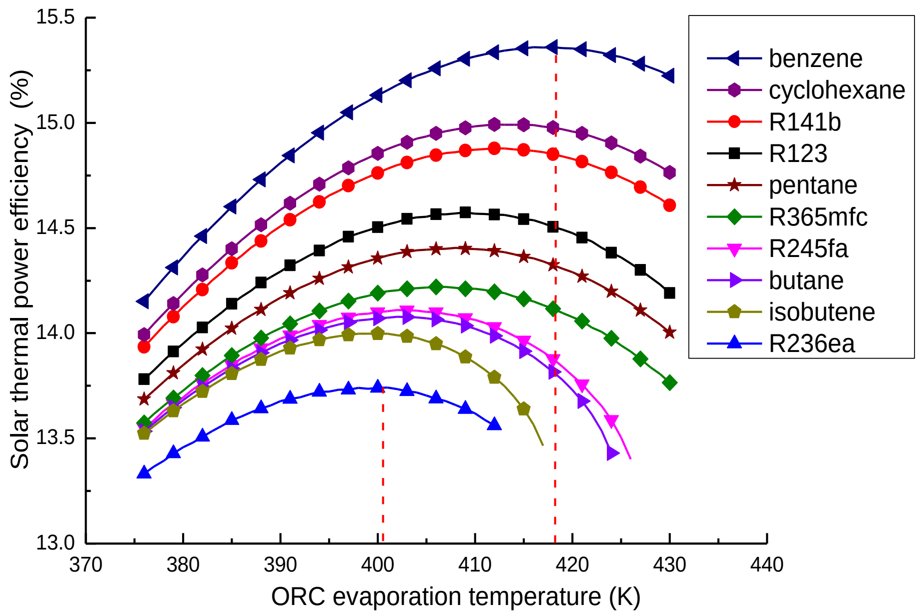

Fig. 11. Variation of solar thermal power efficiency with T_5 when $r_{v,b}$ is 5 and T_H is 523 K.

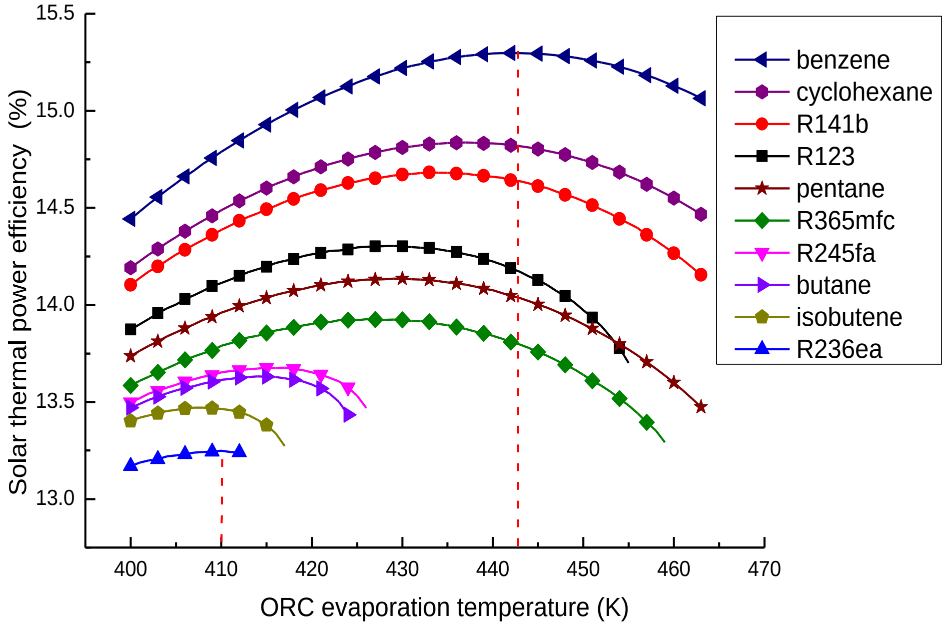

Fig. 12. Variation of solar thermal power efficiency with T_5 when $r_{v,b}$ is 5 and T_H is 573 K.

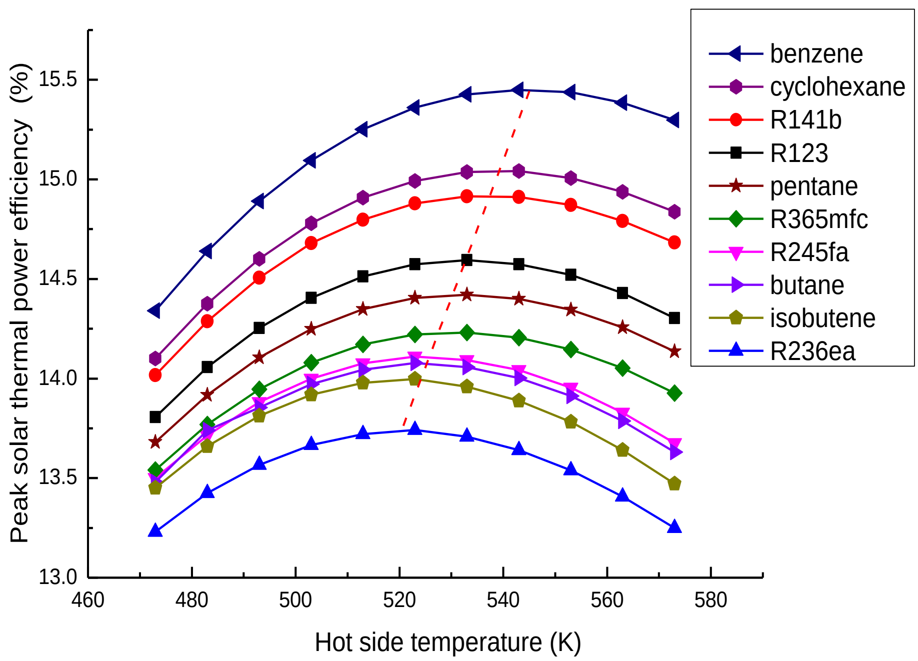

Fig. 13. Variation of peak solar thermal power efficiency with T_H when $r_{v,b}$ is 5.

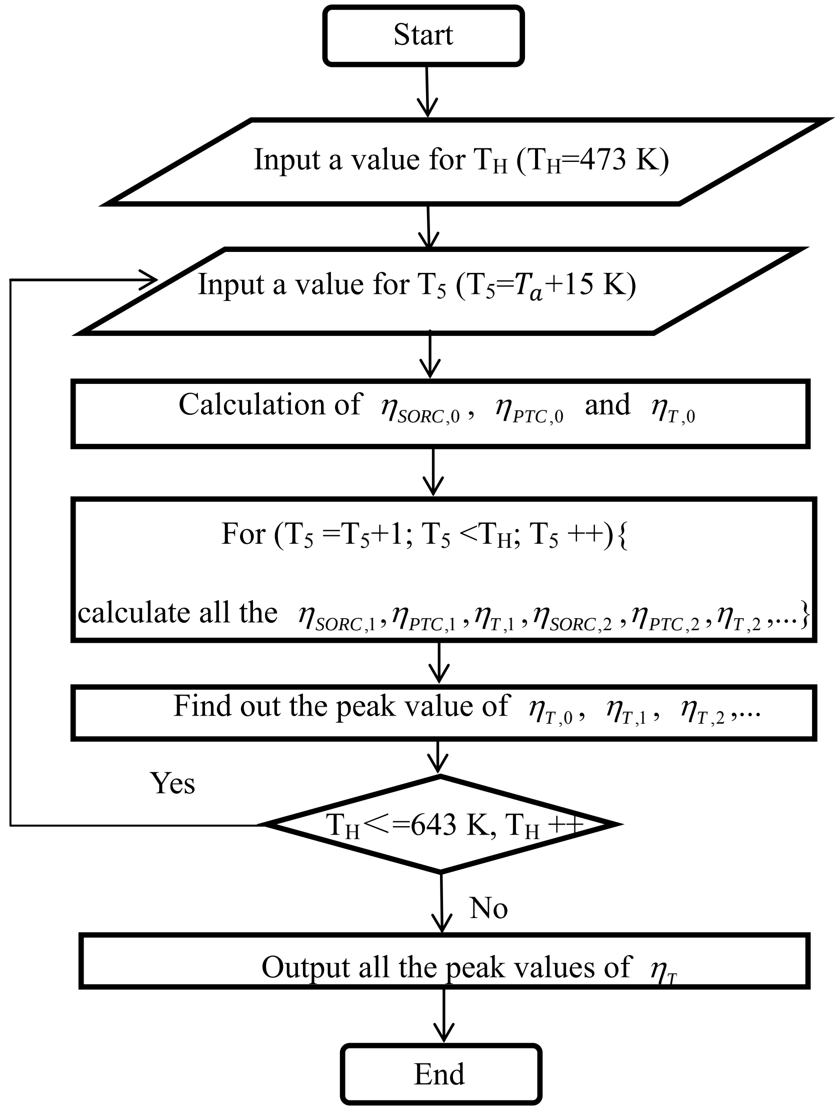

Fig. 14. Determination of peak solar thermal power efficiency with T_H.

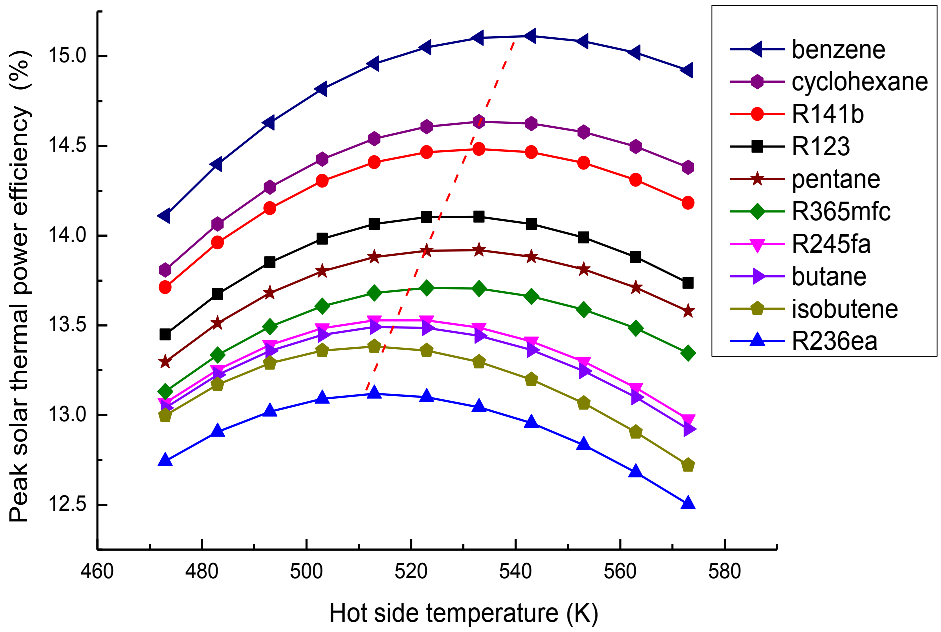

Fig. 15. Variation of peak solar thermal power efficiency with T_H when $r_{v,b}$ is 3.5.

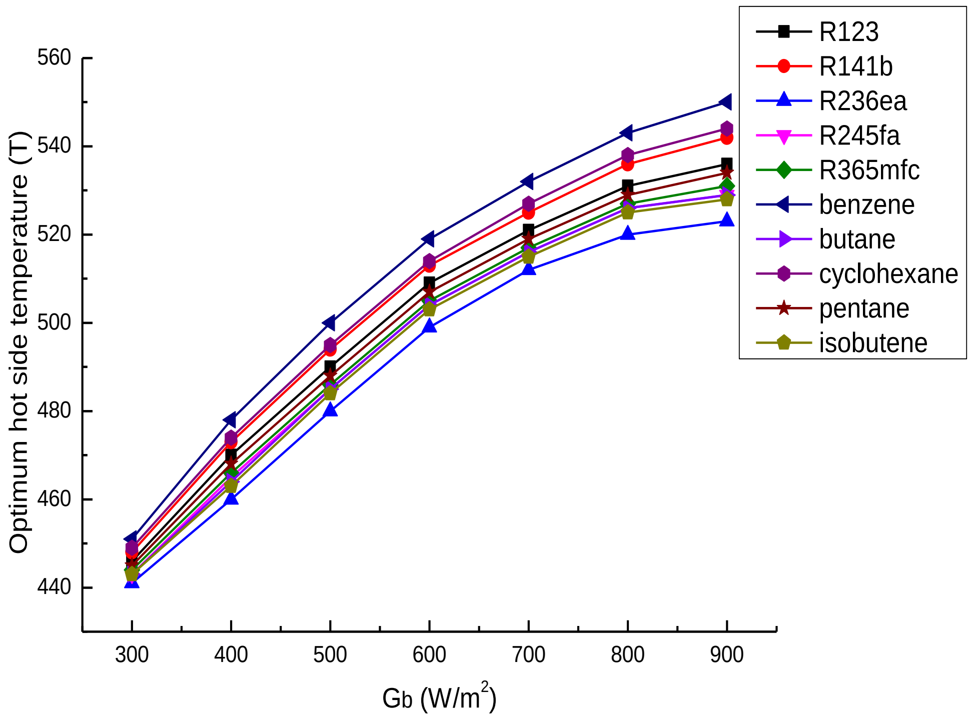

Fig. 16. Variation of optimum hot side temperature with G_b when $r_{v,b}$ is 5.

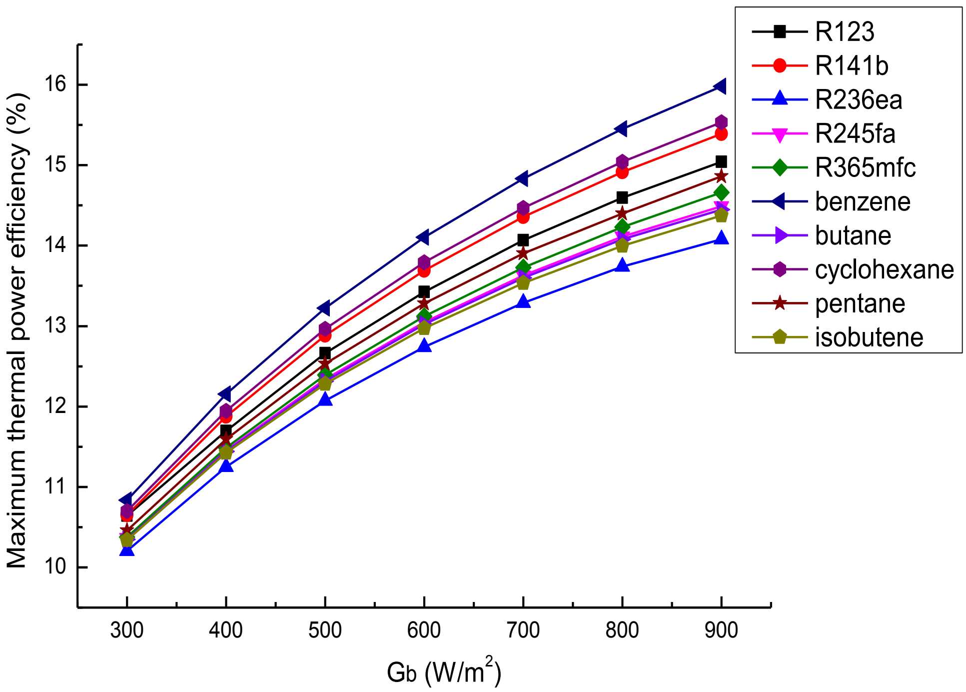

Fig. 17. Variation of maximum solar thermal power efficiency with G_b when $r_{v,b}$ is 5.

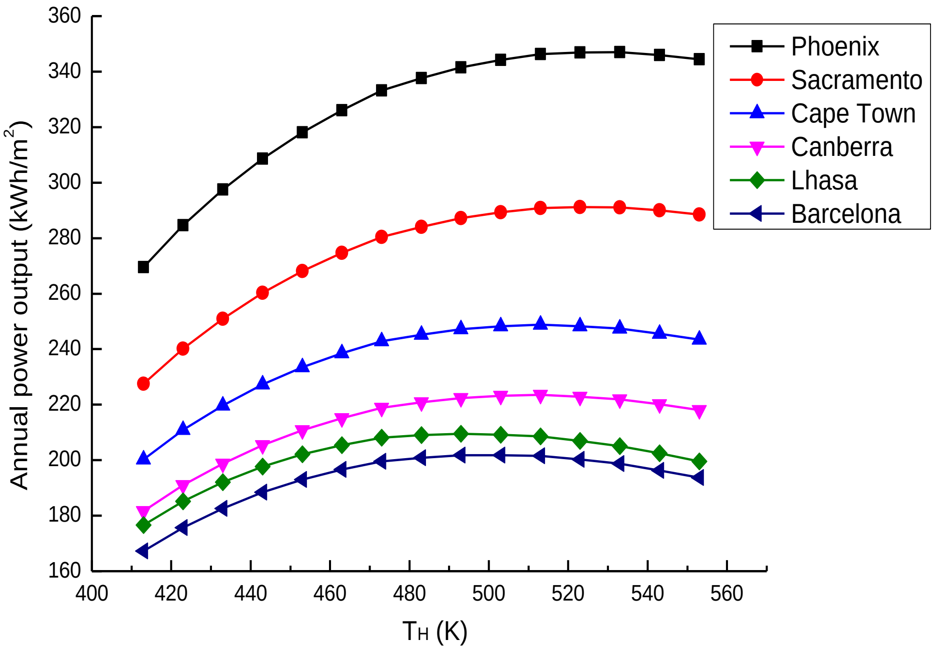

Fig. 18. Annual output of the solar thermal electric power generation with T_H.

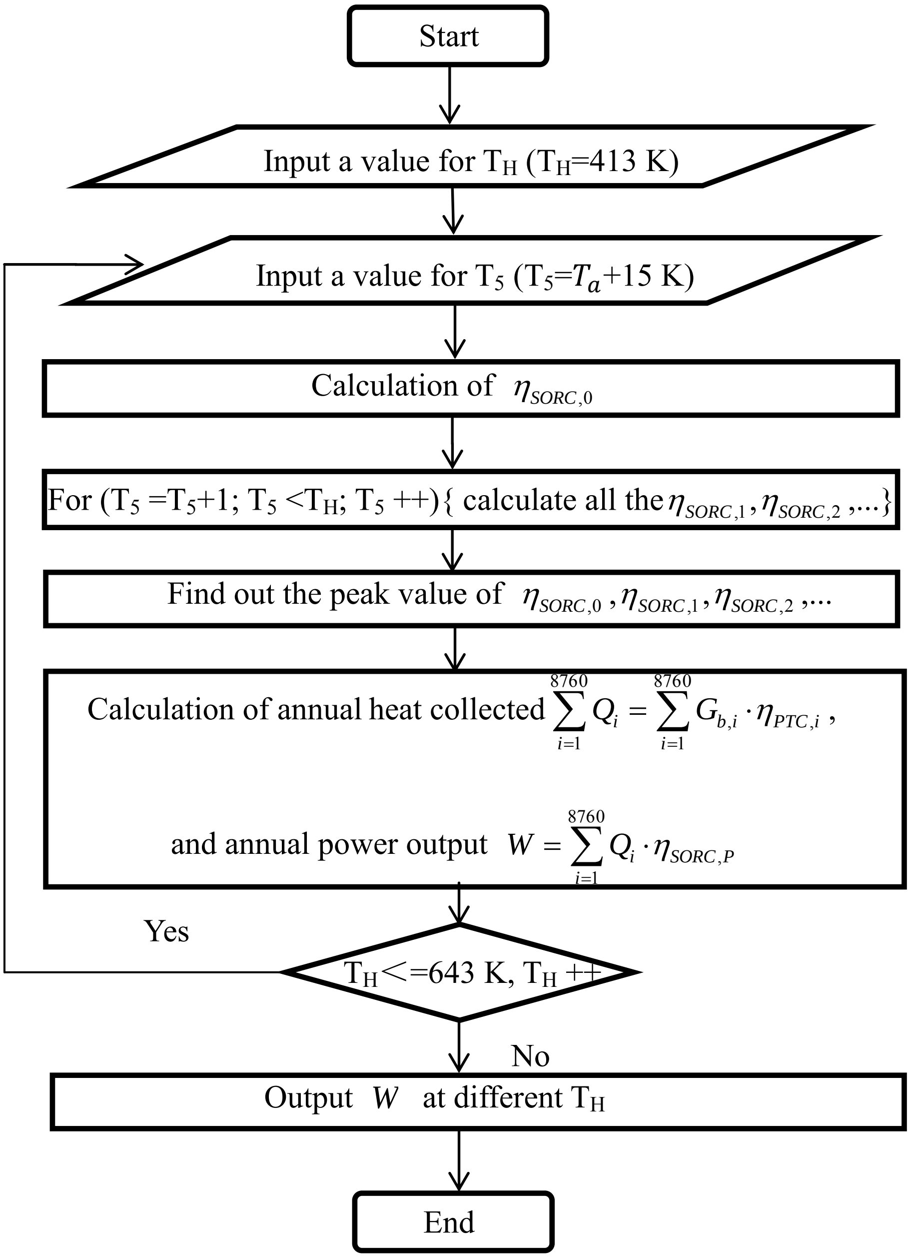

Fig. 19. Determination of maximum annual power output with T_H.

Table 1. Fixed parameters for calculation.

Term	Value
Pinch-point temperature difference, T_{pp}	5 K
Pump efficiency, ε_p	0.8
Peak isentropic efficiency of SE, $\varepsilon_{os,p}$	0.75
Turbine isentropic efficiency, ε_T	0.75
Generator efficiency, ε_g	0.95

Nomenclature			
A	aperture area, m^2	a	ambient
G	solar radiation , W/m^2	b	binary phase/ beam/ built-in
h	enthalpy, kJ/kg	C	cold side
m	mass flow rate, kg/s	ch	characteristic
P	pressure, MPa	D	diagram
Q	hat collected, W	F	fricition
r	ratio	g	generator
γ	isentropic index	H	hot side
T	temperature, K	in	inlet
v	specific volume, m^3/kg	l	liquid phase
W	power output, kW	L	leakage
η ,ε	efficiency	M	mechanical
		net	net
Abbreviation		op	optimum
DSG	direct steam generation	os	overall isentropic
HX	heat exchanger	out	outlet
ORC	organic Rankine cycle	p	pressure/ pump
P	pump	P	peak
PCM	phase-change material	pp	pinch-point
PTC	parabolic trough collectors	s	shaft/ isentropic
SE	screw expander	su	supply

SEGS	solar electricity generating system	t	total mass flowrate
SORC	steam-organic Rankine cycle	T	thermal/ turbine
		Th	theoretical
Subscripts		TD	theoretical diagram
Ⅰ， Ⅱ	Cycle Ⅰ， Ⅱ	TI	theoretical isentropic
0	reference state	TM	thermodynamic
1–8	state points	v	volume